Journal of Solid State Chemistry 186 (2012) 58–63

Contents lists available at SciVerse ScienceDirect

Journal of Solid State Chemistry

journal homepage: www.elsevier.com/locate/jssc

New strategy to the controllable synthesis of $CuInS_2$ hollow nanospheres and their applications in lithium ion batteries

Weixin Zhang*, Hui Zeng, Zeheng Yang, Qiang Wang

School of Chemical Engineering, Hefei University of Technology and Anhui Key Laboratory of Controllable Chemical Reaction & Material Chemical Engineering, Hefei, Anhui 230009, People's Republic of China

ARTICLE INFO

Article history:
Received 9 August 2011
Received in revised form
24 November 2011
Accepted 26 November 2011
Available online 4 December 2011

Keywords:
$CuInS_2$
Anode materials
Lithium ion batteries
Hollow nanospheres

ABSTRACT

A new strategy has been presented to the controllable synthesis of $CuInS_2$ hollow nanospheres based on the Cu_2O solid nanospheres as the precursor in the absence of any surfactant. Specifically, the $CuInS_2$ hollow nanospheres result from hydrothermal transformation of the intermediate Cu_7S_4 hollow nanospheres derived from Cu_2O solid nanosphere precursor by the Kirkendall effect in the conversion process. The $CuInS_2$ hollow nanospheres with diameters of about 250 nm are assembly of nanoparticles with an average size of 20–30 nm. The composition, structure, and morphology of the Cu_2O precursor, the Cu_7S_4 intermediate, and final $CuInS_2$ product have been, respectively, characterized by X-ray diffraction (XRD), field-emission scanning electron microscopy (FESEM), and transmission electron microscopy (TEM) with selected area electron diffraction (SAED). Different from investigation of photovoltaic properties, in this work, the as-prepared $CuInS_2$ hollow nanospheres have been explored as anode materials for rechargeable lithium ion batteries. They deliver a large initial discharge capacity of 1144 mAh g^{-1} and exhibit good cycle performance with a discharge capacity of 265 mAh g^{-1} after 20 cycles, which are superior to those of $CuInS_2$ nanoparticles. The suitable surface area and relatively stable structure of the $CuInS_2$ hollow nanospheres play an important role in their enhanced electrochemical performance as anode materials.

1. Introduction

Over the last decade, hollow nano- and microspheres have received considerable attention due to their potential applications in gas sensors, catalysts, lithium ion batteries, and drug-delivery carriers [1–5]. $CuInS_2$ is one of the promising ternary chalcopyrite materials for photovoltaic applications [6–9]. Up to now, several morphologies including nanorods [10–11], nanoacorns [12], foam-like nanocrystallites [13], and hierarchical microarchitectures [14] have been prepared by using solvothermal methods. However, methods for preparing $CuInS_2$ nanostructures with controlled morphologies are still limited and there are only a few reports on the synthesis of $CuInS_2$ hollow nanospheres. For instances, Lu and co-workers [15] used $Cu(CH_3COO)_2 \cdot H_2O$, $In(NO_3)_3 \cdot 4.5H_2O$, and thioacetamide as raw materials and prepared $CuInS_2$ hollow nanospheres with diameters of 80–100 nm via a surfactant (CTAB) assisted refluxing route in ethylene glycol (EG) at 80 °C for 1.5 h. A vesicle-template mechanism was proposed to explain the formation process of the hollow structure, during which amorphous hollow structures were first formed on the surfactant template and then crystallized in the refluxing process. Tang and co-workers [16,17] also reported that $CuInS_2$ hollow microspheres with diameters of about 1 μm could be obtained via a solvothermal method at 180 °C for 24 h with ethanolamine as the solvent and $CuSO_4 \cdot 5H_2O$, $InCl_3 \cdot 4H_2O$, and thiourea as raw materials. It involved the formation of amorphous primary particles followed by an Ostwald ripening process.

In this study, we propose a new strategy to the controllable synthesis of nearly monodispersed $CuInS_2$ hollow nanospheres with uniform Cu_2O solid nanospheres as the precursor in the absence of any surfactant. Specifically, the $CuInS_2$ hollow nanospheres result from hydrothermal transformation of the intermediate Cu_7S_4 hollow nanospheres originated from Cu_2O solid nanosphere precursor due to the Kirkendall effect in the conversion process. This process avoids using organic solvents like oleylamine, triethylene glycol, and so forth. The diameters of $CuInS_2$ hollow nanospheres can be tuned through controlling the sizes of Cu_2O solid nanosphere precursor. Interestingly, in this work, we have explored the potential application of $CuInS_2$ hollow nanospheres as anode materials in lithium-ion batteries. The results indicate that the as-prepared $CuInS_2$ hollow nanospheres exhibit enhanced electrochemical properties including

* Corresponding author. Fax: +86 551 2901450.
E-mail address: wxzhang@hfut.edu.cn (W. Zhang).

0022-4596/$ - see front matter © 2011 Elsevier Inc. All rights reserved.
doi:10.1016/j.jssc.2011.11.042

discharge capacities and cycling performance compared with $CuInS_2$ nanoparticle counterpart, which can be attributed to its hollow structure.

2. Experimental section

All of the chemicals were of analytical grade made in China and used as raw materials without further purification.

2.1. Preparation of Cu_2O solid nanosphere as precursor

The synthesis of Cu_2O nanospheres as the precursor with different diameters was referred to our previous report [18]. The whole reaction was conducted in a beaker at room temperature under constant magnetic stirring. In a typical procedure, 5 g of sucrose and 0.375 g of $CuSO_4 \cdot 5H_2O$ were dissolved in 100 mL of H_2O. Subsequently, 25 mL of ammonia solution (0.04 M) and 25 mL of NaOH solution (0.20 M) were added dropwise into the above solution in turn. After being stirred for 10 min, 50 mL of ascorbic acid solution (0.03 M) was added into the mixture aqueous solution under magnetic stirring. After 1 h, the yellow precipitates were collected by centrifugation, washed thoroughly with distilled water and ethanol, and dried in vacuum at 60 °C for 4 h.

2.2. Preparation of $CuInS_2$ hollow nanospheres

A typical procedure to synthesize $CuInS_2$ hollow nanospheres was performed as follows. 0.108 g of the obtained Cu_2O nanosphere precursor was dispersed in 20 mL of deionized water by ultrasonication. Then 12 mL of Na_2S aqueous solution (0.25 M) was added into the above mixture under magnetic stirring and a dark black precipitation immediately occurred. After being vigorously stirred for 20 min, 6 mL of $InCl_3$ aqueous solution (0.2 M) was added into the mixed aqueous solution under vigorous stirring. Some yellow precipitates occurred. Then the mixture was ultrasonicated for 1 min till a homogeneous suspension was obtained. The suspension was transferred into a 50 mL Teflon-lined stainless steel autoclave. The autoclave was closed and heated at 170 °C for 24 h. After cooling to room temperature, the products were collected by centrifugation, washed with ethanol and distilled water for several times, and then dried in vacuum at 60 °C overnight for further characterization.

2.3. Preparation of $CuInS_2$ nanoparticles

A typical procedure is as follows: 10 mL of $Cu(NO_3)_2$ aqueous solution (0.15 M) were added dropwise into 25 mL of Na_2S aqueous solution (0.25 M) in a beaker under magnetic stirring. After being stirred for 10 min, 10 mL of $InCl_3$ aqueous solution (0.2 M) was added into the mixed aqueous solution under vigorous stirring, then the mixture was ultrasonicated for 5 min till a homogeneous suspension was obtained. The suspension was also transferred into a 50 mL of Teflon-lined stainless steel autoclave and the following operation steps and conditions were the same as those in the synthesis of $CuInS_2$ hollow nanospheres.

2.4. Characterization

The as-prepared samples were characterized by XRD in a Japan Rigaku D/max-γB X-ray diffractometer with a Cu$K\alpha$ radiation source ($\lambda = 1.5418$ Å) operated at 40 kV and 80 mA. Field-emission scanning electron microscopy (FESEM) measurement was taken on a FEI Sirion-200 scanning electron microscope operating at an accelerating voltage of 10 kV. Transmission electron microscopic (TEM) image and the selected area electron diffraction (SAED) patterns were taken on a Hitachi H-800 transmission electron microscope performed at an accelerating voltage of 200 kV.

N_2 adsorption–desorption isotherms were obtained on a Quantachrome NOVA 2200e surface areas and pore size analyzer at liquid nitrogen temperature. The specific surface areas of the samples were calculated following the multi-point BET (Brunauer–Emmett–Teller) procedure, and average pore diameters were calculated using the Barrett–Joyner–Halenda (BJH) method. Before carrying out the measurement, each sample was degassed at 150 °C for more than 4 h.

2.5. Electrochemical characterization

Before battery testing, the $CuInS_2$ hollow nanospheres and $CuInS_2$ nanoparticles were heated at 300 °C in N_2 atmosphere for 5 h in order to remove adsorbed moisture and increase the crystallinity of the $CuInS_2$ samples (see Supporting Information).

The electrochemical properties of the as-prepared samples were characterized by coin-type cells (CR2032) with lithium disks as counter electrodes. A composite electrode was prepared by mixing the $CuInS_2$ powder, carbon black, and polyvinylidene fluoride (PVDF) in weight ratio of 70:20:10 and dissolved in *n*-methyl pyrrolidinone (NMP) solvent. The obtained slurry was then cast onto copper foil with the slurry thickness controlled by a doctor blade coater. After the evaporation of the solvent by a mild heating, the resulted electrode film was subsequently pressed and punched into a circular disk with a diameter of 11 mm. Then the disks were further dried in vacuum at 120 °C for 5 h. Finally, coin-type cells (CR2032) were assembled in an Ar-filled dry glove box. The liquid electrolyte used was 1 M $LiPF_6$ in a 1:1 mixture of ethylene carbonate (EC) and dimethyl carbonate (DMC), and the separator was Celgard 2400 microporous polypropylene membrane. Galvanostatical charge and discharge was measured on a multi-channel battery tester (Neware Battery Test System, Shenzhen Neware Electronic Co., China) between 0.005 and 3 V at 25 °C.

3. Results and discussion

Fig. 1 presents the structure and morphology of Cu_2O precursor for preparing $CuInS_2$. Fig. 1(a) shows the X-ray diffraction (XRD) pattern of the precursor. All of the diffraction peaks can be indexed to the cubic Cu_2O (JCPDS No. 05-0667). The low-magnification FESEM image in Fig. 1(b) displays that it consists of nanospheres with uniform size and good monodispersity. A high-magnification FESEM image in Fig. 1(c) shows that the average diameter of the Cu_2O nanospheres is about 250 nm. Fig. 1(d) and (e) presents TEM images of Cu_2O nanospheres and further confirm that the sample has uniform sphere morphology with diameters of 250 nm. A high-magnification TEM image in Fig. 1(e) indicates that the nanospheres are solid. Such observations are consistent with the FESEM results. The SAED pattern from a single Cu_2O nanosphere in Fig. 1(e) shows concentric diffraction rings, which indicates the polycrystalline nature of the product. The rings can be indexed to (111), (200), (220), and (311) reflections of cubic Cu_2O.

Fig. 2 presents the structure and morphology of the final hydrothermal reaction product $CuInS_2$ based on Cu_2O nanosphere precursor. Fig. 2(a) shows the XRD pattern of the product. All of the diffraction peaks can be well indexed to the tetragonal $CuInS_2$ (JCPDS No. 85-1575). The impurities such as Cu_7S_4 or In_2S_3 could not be observed. The low-magnification FESEM image in Fig. 2(b) shows that $CuInS_2$ has the similar morphology to that of the Cu_2O nanosphere precursor. A high-magnification FESEM image in Fig. 2(c) clearly shows that the average diameter of $CuInS_2$ hollow

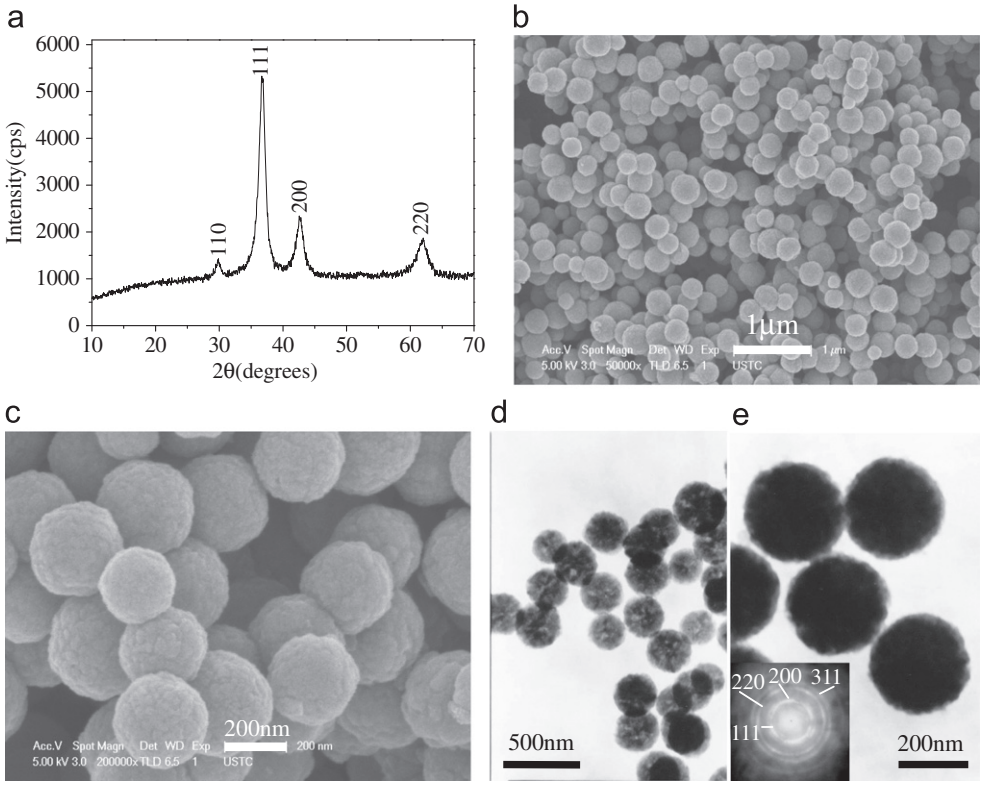

Fig. 1. (a) XRD pattern, (b, c) FESEM images, and (d, e) TEM images of as-prepared Cu_2O precursor. Inset of (e): SAED pattern of an individual nanosphere.

nanospheres is about 250 nm. A typical broken sphere is shown in Fig. 2(c), which clearly indicates the hollow structure of the obtained $CuInS_2$ nanospheres. It can be seen that the shell of $CuInS_2$ hollow nanospheres is assembly of small nanoparticles with an average size of 20–30 nm. The TEM images of the $CuInS_2$ product in Fig. 2(d) and (e) show that all of the nanospheres have a strong contrast difference between the shell (dark) and center (light), suggesting that the nanospheres have hollow structure. A high-magnification TEM image in Fig. 2(e) shows that the average diameter of $CuInS_2$ hollow nanospheres is about 250 nm, which indicates that the surface of $CuInS_2$ nanosphere is not smooth. Such observations are consistent with the FESEM results. The SAED pattern in Fig. 2(e) shows concentric diffraction rings indicating the polycrystalline nature of the product. The rings can be indexed to (112), (220), and (116) reflections of $CuInS_2$. It further confirms that the shell of the $CuInS_2$ hollow nanospheres are constructed from small $CuInS_2$ nanoparticles. Furthermore, energy-dispersive X-ray spectrometry (EDX) was also used to determine the local chemical composition of the product. A typical EDX spectrum in Fig. 2(f) reveals that the sample is mainly composed of Cu, In, and S elements. Silicon peak comes from the silicon substrate for the sample. Oxygen peak in the spectrum probably originates from the unavoidable surface adsorption of oxygen onto the samples from exposure to air during sample processing. The average atomic ratio of Cu/In/S is about 1.1:0.9:1.9, which is close to the stoichiometry of $CuInS_2$, in agreement with the above XRD results.

To understand the formation mechanism of $CuInS_2$ hollow nanospheres, the intermediate product has to be characterized when Cu_2O reacts with Na_2S solution in atmosphere at room temperature for 20 min. The XRD pattern of it can be indexed to the monoclinic Cu_7S_4 (JCPDS No. 23-0958) as shown in Fig. S1(a) (Supporting Information). TEM image in Fig. S1(b) displays that Cu_7S_4 exists in hollow nanospheres with similar average diameter of about 250 nm to that of Cu_2O solid nanosphere precursor. Here, the formation of hollow Cu_7S_4 nanospheres from Cu_2O nanospheres is believed to be much related with the Kirkendall effect [19–22].

The TEM images of the morphology evolution after Cu_2O nanospheres reacted with Na_2S solution (0.25 M) for different time are shown in Fig. S2 (Supporting Information). When Cu_2O nanospheres react with Na_2S solution, a layer of Cu_7S_4 would first form on the surface of Cu_2O nanosphere, separating the inner Cu^+ ions from outer S^{2-} ions. The relatively large difference in concentration of Cu^+ ions as well as S^{2-} ions between core and solution provides a great driving force for Cu^+ ions diffusing outward and S^{2-} ions inward. Then, due to the larger diffusion rate of Cu^+ than S^{2-} through the Cu_7S_4 layer, the void within particles is gradually formed till Cu_7S_4 hollow nanospheres are formed. When hollow Cu_7S_4 nanospheres react with $InCl_3$ solution at 170 °C for 24 h hydrothermally, the reaction takes place on the shell of the hollow nanospheres to form $CuInS_2$ product, which keeps the hollow nanosphere morphology as well.

For comparison, $CuInS_2$ nanoparticles have been prepared by the hydrothermal method. The diffraction peaks of the XRD pattern in Fig. 3(a) can be well indexed to the tetragonal $CuInS_2$ (JCPDS No. 85-1575). The TEM image in Fig. 3(b) shows that the average particle size is about 20–30 nm. The SAED pattern in Fig. 3(b) shows concentric diffraction rings from nanoparticles, which indicates the polycrystalline nature of the product. The rings can be indexed to (112), (220), and (116) reflections of $CuInS_2$.

Nitrogen adsorption–desorption isotherms and the corresponding pore-size distributions of the as-synthesized $CuInS_2$ hollow nanospheres and $CuInS_2$ nanoparticles are shown in Fig. 4. The BET surface area of $CuInS_2$ hollow nanospheres was 7.43 $m^2\,g^{-1}$ and that of $CuInS_2$ nanoparticles was 21.31 $m^2\,g^{-1}$. The corresponding average pore diameters were 4.8 nm and 9.1 nm, according to the BJH model calculated from the nitrogen isotherms of the two $CuInS_2$ samples. The BET surface area of $CuInS_2$ hollow nanospheres

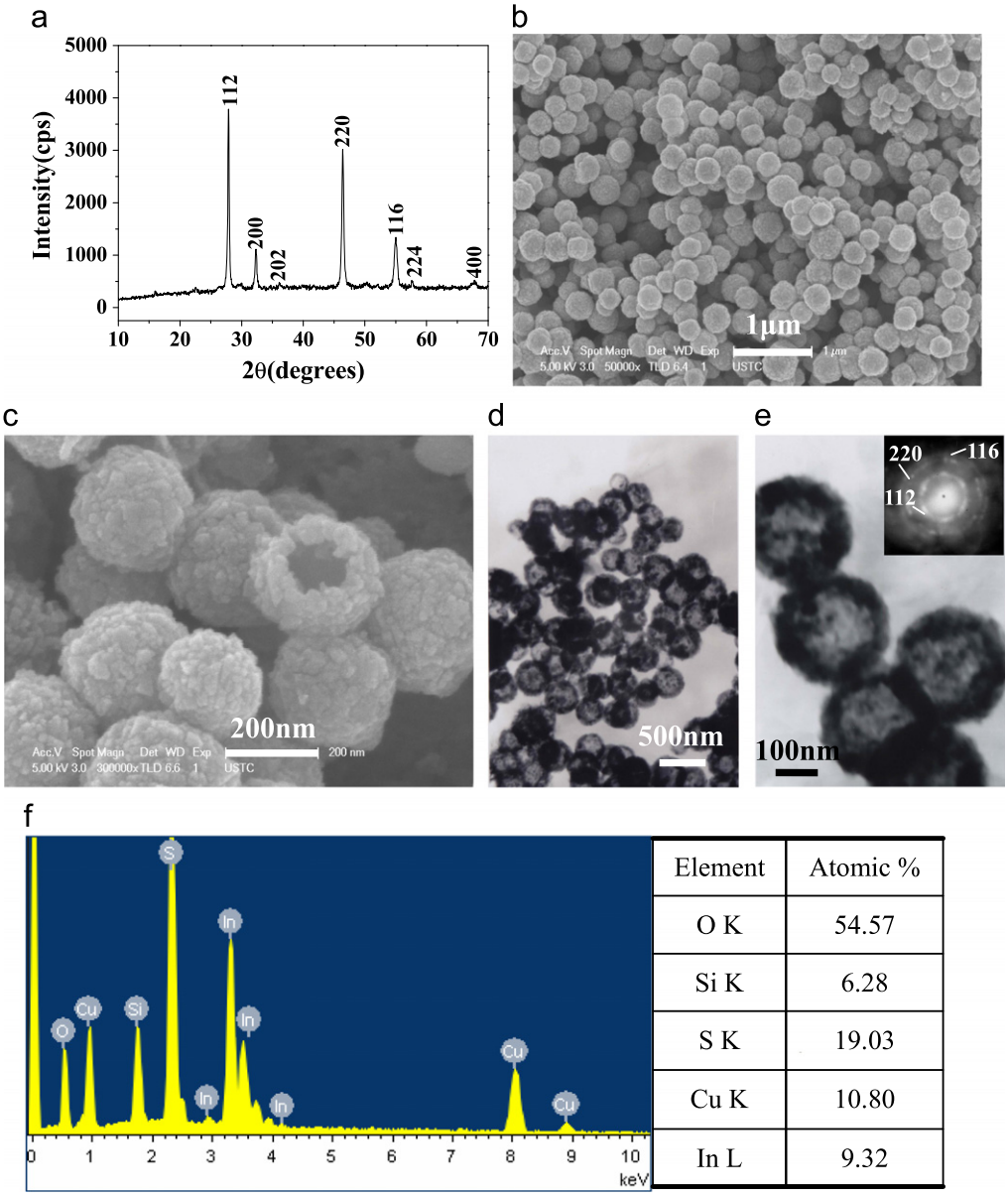

Fig. 2. (a) XRD pattern, (b, c) FESEM images, (d, e) TEM images, and (f) EDX spectrum of the as-prepared $CuInS_2$ hollow nanospheres. Inset of (e): SAED pattern of an individual hollow nanosphere.

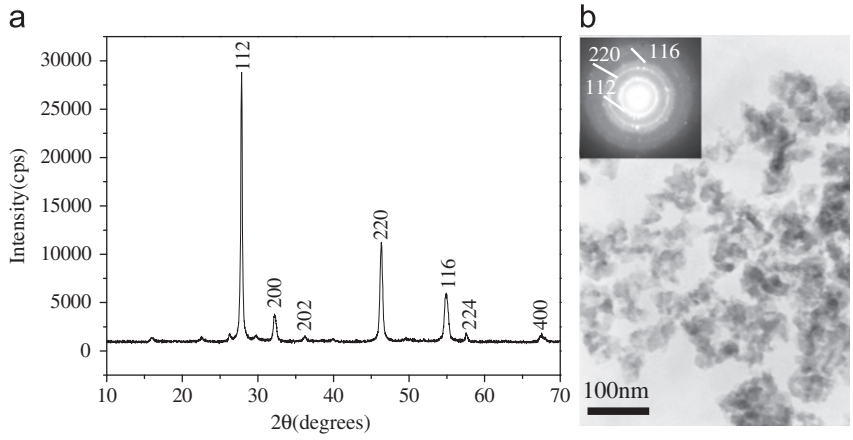

Fig. 3. (a) XRD pattern and (b) TEM image of as-prepared $CuInS_2$ nanoparticles. Inset of (b): SAED pattern of nanoparticle.

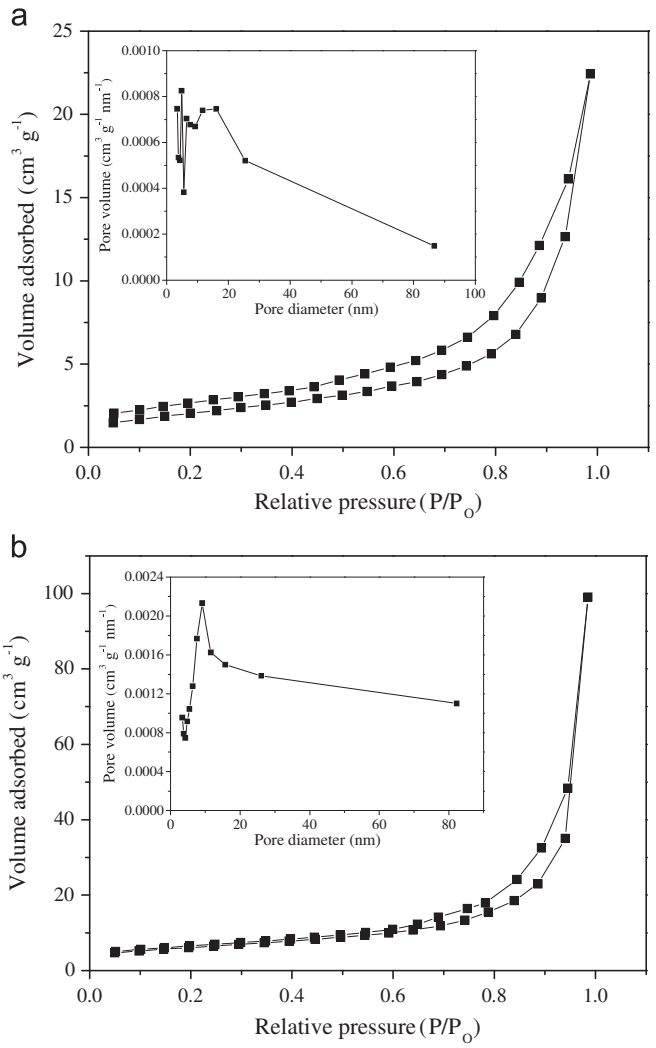

Fig. 4. N_2 adsorption–desorption isotherm curves of (a) $CuInS_2$ hollow nanospheres and (b) $CuInS_2$ nanoparticles. The insets present the corresponding pore-size distributions of (a) $CuInS_2$ hollow nanospheres and (b) $CuInS_2$ nanoparticles.

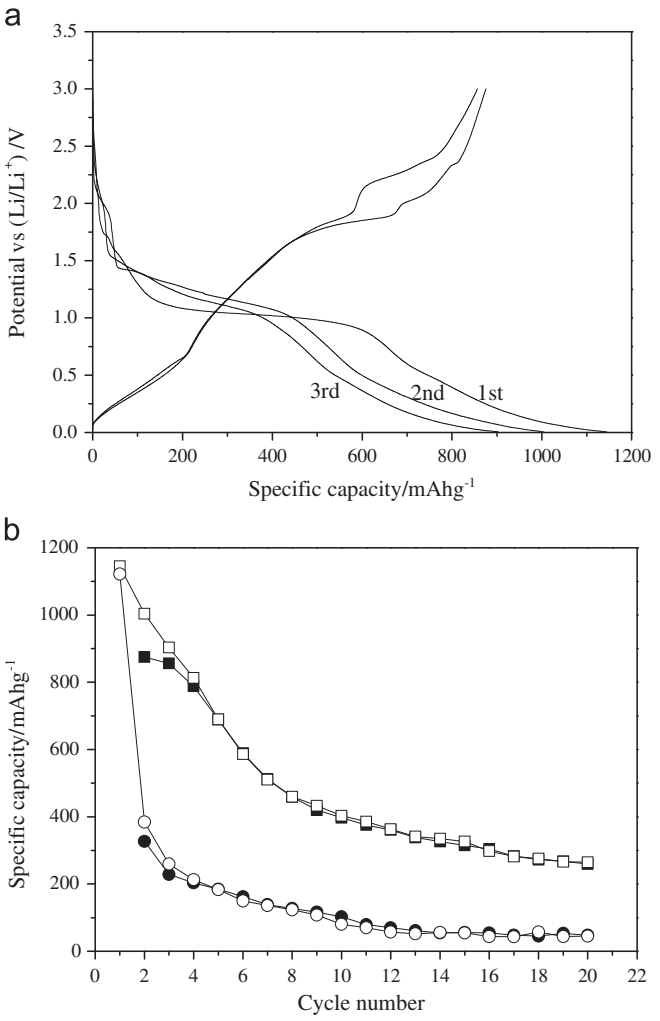

Fig. 5. (a) Discharge and charge curves of the $CuInS_2$ hollow nanospheres for the first three cycles, and (b) specific capacity as a function of cycle number and discharge (open symbols) or charge (filled symbols) for electrodes fabricated from $CuInS_2$ hollow nanospheres (□, ■) and $CuInS_2$ nanoparticles (○, ●), respectively. In each case, the measurements were taken at a current density of 30 mA g^{-1} between the voltage range of 3–0.005 V.

is smaller than the nanoparticles, which is much related with their morphologies. Because the shell of $CuInS_2$ hollow nanospheres is assembly of nanoparticles, which have smaller interface area to some extent in comparison with $CuInS_2$ nanoparticles.

$CuInS_2$ is well-known for its photovoltaic property. In this work, the electrochemical performances of the two $CuInS_2$ samples with different morphologies have been investigated. Before battery testing, the hollow nanospheres and nanoparticles were heated at 300 °C in N_2 atmosphere for 5 h to remove the trapped and adsorbed moisture. Fig. S3(a) (Supporting Information) shows the XRD pattern of $CuInS_2$ hollow nanospheres after the post-treatment, which indicates the same tetragonal $CuInS_2$ as shown in Fig. 2(a) but with higher intensities due to higher crystallization. The TEM image in Fig. S3(b) (Supporting Information) also displays that the post-treated $CuInS_2$ has retained the morphology of hollow nanospheres.

Fig. 5(a) shows the discharge and charge curves of the $CuInS_2$ hollow nanospheres for the first three cycles at a current density of 30 mA g^{-1} between the voltage range of 3–0.005 V. The initial discharge capacity of $CuInS_2$ hollow nanospheres was 1144 mAh g^{-1}, with a second discharge capacity of 1004 mAh g^{-1} and a third discharge capacity of 903 mAh g^{-1}. For comparison, the electrochemical performance of $CuInS_2$ nanoparticles was also tested at the same condition. The discharge and charge curves (Fig. S4 in the Supporting Information) of the $CuInS_2$ nanoparticles indicate that the initial discharge capacity of $CuInS_2$ nanoparticles was 1122 mAh g^{-1}, with a second discharge capacity of 384 mAh g^{-1} and a third discharge capacity of 260 mAh g^{-1}. $CuInS_2$ hollow nanospheres have the similar value of the initial discharge capacity to that of $CuInS_2$ nanoparticles. Because $CuInS_2$ hollow nanospheres is actually assembly of nanoparticles, which can enhance surface electrochemical reactivity and lead to increase in the capacity of the initial discharge [23,24].

The cycle performances of $CuInS_2$ hollow nanospheres and $CuInS_2$ nanoparticles at a current density of 30 mA g^{-1} are shown in the Fig. 5(b). The discharge capacity of $CuInS_2$ hollow nanospheres was 265 mAh g^{-1} after 20 cycles, but the discharge capacity of $CuInS_2$ nanoparticles dropped to 48 mAh g^{-1} after 20 cycles. Combined with their BET surface area results, $CuInS_2$ nanoparticles have higher surface area than hollow nanospheres. Obviously, the $CuInS_2$ nanoparticles with higher surface area will provide higher electrolyte/electrode surface area and may lead to more significant side reactions between the electrode material and electrolyte, such as the formation of thicker SEI films, which will consume more lithium ions and result in larger irreversible capacity [25,26]. In addition, the hollow nanosphere structure

may accommodate the strain stress of the volume change during the charge–discharge process, which will alleviate the pulverization of particles and promote its cycling performance superior to the nanoparticles [26,27].

In order to observe the morphology change of the $CuInS_2$ hollow nanospheres after 30 charge and discharge cycles. The cells after 30 charge and discharge cycles were disassembled according to references [28] in an Ar-filled dry glove box and the working electrode was taken out. The working electrode was immersed into dimethyl carbonate (DMC) and n-methyl pyrrolidinone (NMP) to remove the electrolyte and polyvinylidene fluoride (PVDF), respectively. Finally, the black powder was collected by centrifugation, washed with ethanol and distilled water for several times, and then dried in vacuum at 60 °C for 4 h.

Fig. S5 (Supporting Information) shows the FESEM images of the electrode material recovered after 30 charge and discharge cycles. It can be found that some complete hollow nanospheres still exist in the mixture of the recovered electrode material, which has undergone such processes as preparation of the electrode, 30 charge–discharge cycling, and recovery of the electrode material. It implies that the $CuInS_2$ hollow nanospheres can retain their morphology fairly well during the charge–discharge process, although some broken hollow nanospheres are present in the mixture, which may result from the other two processes. Many small nanoparticles may be directly from the carbon black added in the mixture during electrode preparation.

Based on the above experimental results and analysis, it can be concluded that $CuInS_2$ hollow nanospheres can enhance the electrochemical performance owning to its suitable surface area and stable structure compared with the nanoparticles.

4. Conclusions

In summary, we have successfully synthesized $CuInS_2$ hollow nanospheres via a new approach by using the self-prepared Cu_2O solid nanospheres as the precursor in the absence of any surfactant. The $CuInS_2$ hollow nanospheres with diameter of about 250 nm are assembly of nanoparticles with an average size of 20–30 nm. This synthesis strategy has been demonstrated to be an efficient and controllable route to ternary sulfide hollow nanostructures. As an anode material for rechargeable lithium ion batteries, the $CuInS_2$ hollow nanospheres exhibit enhanced electrochemical performances compared with $CuInS_2$ nanoparticles. They deliver a large initial discharge capacity of 1144 mAh g^{-1} and exhibit good cycle performance with a discharge capacity of 265 mAh g^{-1} after 20 cycles. The suitable surface area and relatively stable structure of the $CuInS_2$ hollow nanospheres are considered to be the main reason for the enhanced electrochemical performance.

Acknowledgments

This work has been supported by the National Natural Science Foundation of China (NSFC Grants 20871038, 20976033, and 21176054), the Fundamental Research Funds for the Central Universities (2010HGZY0012), and the Education Department of Anhui Provincial Government (TD200702).

Appendix A. Supplementary material

Supplementary data associated with this article can be found in the online version at doi:10.1016/j.jssc.2011.11.042.

References

[1] X.L. Li, T.J. Lou, X.M. Sun, Y.D. Li, Inorg. Chem. 43 (2004) 5442.
[2] L. Kong, X. Lu, X. Bian, W. Zhang, C. Wang, J. Solid State Chem. 183 (2010) 2421.
[3] Y.D. Yin, Y. Lu, B. Gates, Y.N. Xia, Chem. Mater. 13 (2001) 1146.
[4] Y.F. Zhu, E. Kockrick, T. Ikoma, N. Hanagata, S. Kaskel, Chem. Mater. 21 (2009) 2547.
[5] F. Tao, C. Gao, Z. Wen, Q. Wang, J. Li, Z. Xu, J. Solid State Chem. 182 (2009) 1055.
[6] K. Yoshino, T. Ikari, S. Shirakata, H. Miyake, K. Hiramatsu, Appl. Phys. Lett. 78 (2001) 742.
[7] B.D. Weil, S.T. Connor, Y. Cui, J. Am. Chem. Soc. 132 (2010) 6642.
[8] L. Li, N. Coates, D. Moses, J. Am. Chem. Soc. 132 (2010) 22.
[9] E. Arici, N.S. Sariciftci, D. Meissner, Adv. Funct. Mater. 13 (2003) 165.
[10] Y. Jiang, Y. Wu, X. Mo, W.C. Yu, Y. Xie, Y.T. Qian, Inorg. Chem. 39 (2000) 2964.
[11] S.T. Connor, C.M. Hsu, B.D. Weil, S. Aloni, Y. Cui, J. Am. Chem. Soc. 131 (2009) 4962.
[12] S.H. Choi, E.G. Kim, T. Hyeon, J. Am. Chem. Soc. 128 (2006) 2520.
[13] G.Z. Shen, D. Chen, K.B. Tang, Z. Fang, J. Sheng, Y.T. Qian, J. Cryst. Growth 254 (2003) 75.
[14] L. Zheng, Y. Xu, Y. Song, C.Z. Wu, M. Zhang, Y. Xie, Inorg. Chem. 48 (2009) 4003.
[15] A.Y. Zhang, Q. Ma, M.K. Lu, G.W. Yu, Y.Y. Zhou, Z.F. Qiu, Cryst. Growth Des. 8 (2008) 2402.
[16] Y.X. Qi, K.B. Tang, S.Y. Zeng, W.W. Zhou, Micropor. Mesopor. Mater 114 (2008) 395.
[17] Y.X. Qi, Q.C. Liu, K.B. Tang, Z.H. Liang, Z.B. Ren, X.M. Liu, J. Phys. Chem. C 113 (2009) 3939.
[18] Z.H. Yang, D.P. Zhang, W.X. Zhang, M. Chen, J. Phys. Chem. Solids 70 (2009) 840.
[19] Y.D. Yin, R.M. Rioux, C.K. Erdonmez, S. Hughes, G.A. Somorjai, A.P. Alivisatos, Science 304 (2004) 711.
[20] Y.L. Wang, L. Cai, Y.N. Xia, Adv. Mater. 17 (2005) 473.
[21] J. Xu, Y.B. Tang, W.X. Zhang, C.S. Lee, Z.H. Yang, S.T. Lee, Cryst. Growth Des. 9 (2009) 4524.
[22] W.X. Zhang, C.Y. Luan, Z.H. Yang, X.T. Liu, D.P. Zhang, S.H. Yang, Appl. Surf. Sci. 253 (2007) 6063.
[23] P. Poizot, S. Laruelle, S. Grugeon, L. Dupont, J.M. Tarascon, Nature 407 (2000) 496.
[24] S. Laruelle, S. Grugeon, P. Poizot, M. Dollé, L. Dupont, J.M. Tarascon, J. Electrochem. Soc. 149 (2002) A627.
[25] P.G. Bruce, B. Scrosati, J.M. Tarascon, Angew. Chem. Int. Ed. 47 (2008) 2930.
[26] Y.G. Guo, J.S. Hu, L.J. Wan, Adv. Mater. 20 (2008) 2878.
[27] S.Q. Wang, J.Y. Zhang, C.H. Chen, Scr. Mater. 57 (2007) 337.
[28] D.W. Zhang, C.H. Chen, J. Zhang, F. Ren, Chem. Mater. 17 (2005) 5242.